QUANTIFYING THE EFFECTS OF THE ELECTRODE–BRAIN INTERFACE ON THE CROSSING ELECTRIC CURRENTS IN DEEP BRAIN RECORDING AND STIMULATION

N. YOUSIF,[a] R. BAYFORD,[b] S. WANG[c] AND X. LIU[a,d]*

[a]*The Movement Disorders and Neurostimulation Unit, Department of Clinical Neuroscience, Division of Neuroscience and Mental Health, Faculty of Medicine, Imperial College London, 10 East, Charing Cross Hospital, Fulham Palace Road, London W6 8RF, UK*

[b]*The Bio-modelling/Bio-informatics Group, Department of Natural Science, Institute of Social and Health Research, Middlesex University, London, UK*

[c]*Department of Physiology, Anatomy and Genetics, University of Oxford, Oxford, UK*

[d]*The Movement Disorders and Neurostimulation Unit, Department of Neuroscience, Charing Cross Hospital, London, UK*

Abstract—A depth electrode–brain interface (EBI) is formed once electrodes are implanted into the human brain. We investigated the impact of the EBI on the crossing electric currents during both deep brain recording (DBR) and deep brain stimulation (DBS) over the acute, chronic and transitional stages post-implantation, in order to investigate and quantify the effect which changes at the EBI have on both DBR and DBS. We combined two complementary methods: (1) physiological recording of local field potentials via the implanted electrode in patients; and (2) computational simulations of an EBI model. Our depth recordings revealed that the physiological modulation of the EBI in the acute stage via brain pulsation selectively affected the crossing neural signals in a frequency-dependent manner, as the amplitude of the electrode potential was inversely correlated with that of the tremor-related oscillation, but not the beta oscillation. Computational simulations of DBS during the transitional period showed that the shielding effect of partial giant cell growth on the injected current could shape the field in an unpredictable manner. These results quantitatively demonstrated that physiological modulation of the EBI significantly affected the crossing currents in both DBR and DBS. Studying the microenvironment of the EBI may be a key step in investigating the mechanisms of DBR and DBS, as well as brain–computer interactions in general. © 2008 IBRO. Published by Elsevier Ltd. All rights reserved.

Key words: local field potentials, computational simulation, finite element model.

*Correspondence to: X. Liu, The Movement Disorders and Neurostimulation Unit, Department of Clinical Neuroscience, Division of Neuroscience and Mental Health, Faculty of Medicine, Imperial College London, 10 East, Charing Cross Hospital, Fulham Palace Road, London W6 8RF, UK. Tel: +44-208-8467631; fax: +44-208-3830663.
E-mail address: x.liu@ic.ac.uk (X. Liu).
Abbreviations: BP, blood pressure; DBR, deep brain recording; DBS, deep brain stimulation; EBI, electrode–brain interface; ECF, extracellular fluid; FEM, finite element method; GP, globus pallidus; LFP, local field potential; MRI, magnetic resonance imaging; PVG, periventricular gray; STFT, short-time Fourier transform; STN, subthalamic nucleus.

Since the early 1990s, there has been a revival of therapeutic deep brain stimulation (DBS) to treat movement disorders (Benabid et al., 1987, 1994, 2002; Vitek, 2002; Vidailhet et al., 2005; Deuschl et al., 2006; Kupsch et al., 2006), neuropathic pain (Young and Chambi, 1987; Kumar et al., 1997; Bittar et al., 2005), epilepsy (Hodaie et al., 2002; Kerrigan et al., 2004) and psychiatric disorders (Nuttin et al., 2003; Mayberg et al., 2005). This treatment involves the unilateral or bilateral implantation of metal electrode(s) into selected brain areas, through which electrical pulses are delivered to modulate neuronal activity and alleviate abnormal symptoms. Implanted electrodes also provide an invaluable opportunity to obtain high quality information about the synchronized population activity from the depth structures of the brain (deep brain recording, DBR), in the form of local field potentials (LFPs). This can reveal the pathological mechanisms at the population level (Engel et al., 2005; Liu et al., 2006; Wang et al., 2006; Brown et al., 2006), as well as the modulation of this pathophysiology by either medication (Brown et al., 2001; Priori et al., 2004; Doyle et al., 2005; Brown and Williams, 2005; Kuhn et al., 2006; Marceglia et al., 2006), or electrical stimulation (Brown et al., 2004; Priori et al., 2006; Foffani et al., 2006; Wingeier et al., 2006).

It is well established that an exchange of ions and electrons occurs between a metal electrode and the natural or artificial fluid at the electrode–tissue interface, thereby forming an electrical double layer (Rockwood, 1986). However, only recently has the depth electrode–brain interface (EBI) been studied in the case of DBS (Butson and McIntyre, 2005; Xie et al., 2006; Yousif et al., 2007). The functional compartments of a broad depth EBI can be defined as consisting of (1) the implanted depth electrode; (2) the surrounding brain tissue; and (3) a peri-electrode space, which is filled with extracellular fluid (ECF) at the acute stage a few days post-implantation (Thoma et al., 1987), and is replaced by giant cell growth (Moss et al., 2004) or the formation of microglia (Griffith and Humphrey, 2006) at the chronic stage. This encapsulation process is stabilized over a period of 6–8 weeks post-implantation. These observations indicate that the EBI evolves over time.

The clear significance of studying the biophysical properties of the EBI is that the changes in such properties will affect the electric current crossing the interface during both recording and stimulation procedures. This can be a key step in improving the signal to noise ratio of depth recording, investigating the mechanisms of therapeutic DBS, and optimizing the stimulation parameter settings. We previ-

ously demonstrated (Xie et al., 2006) using LFP recordings, that in the acute stage post-implantation an electrode potential reflecting the electrical charge established following the exchange of ions and electrons, was modulated by physiological brain pulsation. We postulated that this is due to two factors: 1) the relative motion between the pulsating brain and the implanted electrode; 2) the pressure on the electrode which is varying with heart rate. The physiologically modulated electrode potentials could be identified as a specific component in the recorded compound LFP signals that were time-locked with blood pressure (BP) signals (Xie et al., 2006). Further supporting evidence that the electrode potential is modulated by brain pulsation came from another study of the acute after-stimulation effects of subthalamic nucleus (STN) stimulation for the treatment of Parkinson's disease (Priori et al., 2006). This study showed that the magnitude of such electrical charges could be dramatically enhanced during DBS, possibly as the ECF is further polarized by the injected electrical current, and gradually declined following the stimulation being turned off.

Recently, a number of computational modeling studies (McIntyre et al., 2004; Hemm et al., 2005a,b; Gimsa et al., 2006; Butson et al., 2007; Sotiropoulos and Steinmetz, 2007) have been carried out using the finite element method (FEM, for a general reference see Zienkiewicz et al., 2005) to compensate for the present impossibility of measuring the spread of current directly in the depth structures of the human brain (Yousif and Liu, 2007a). However, future advances, for example in voltage sensitive dye techniques, may advance our understanding of the effects of stimulation on cortical activity (Hillman, 2007). Using a model of the generic depth EBI which is independent of the cellular structure of the surrounding brain tissue, the neu-

rological disorder treated, and the instrumentation used (Moss et al., 2004; Xie et al., 2006), our quantitative simulations (Yousif et al., 2007) revealed that the peri-electrode space was a significant element of the EBI and was modulated by physiological factors including brain pulsation in the acute stage, and the growth of giant cells in the chronic stage.

A number of questions remain about the EBI. Firstly, no quantitative evidence has been reported on the effect of physiological modulation of the EBI on LFP recordings; and secondly, there is a transitional period within the initial 2–8 weeks post-implantation, during which the peri-electrode space gradually changes from being filled with ECF, to partial encapsulation which occurs as early as 2 weeks, and is followed by the stabilization of the growth of reactive giant cells after 6–8 weeks (Moss et al., 2004). The changes occurring during this transitional period are crucial for adjusting stimulation parameters in DBS, and yet have not been investigated extensively, as neurophysiological examination after the initial acute stage is not possible. This is because LFP recordings can only be made while the implanted electrodes are "externalized" in the first few days post-implantation (Liu, 2003), and magnetic resonance imaging (MRI) of DBS has limited resolution on the peri-electrode space due to significant artifact of the metal electrode contacts (Fig. 1; Pollo et al., 2004). In the current study, we hypothesize that the changes in the peri-electrode space occurring over the acute, transitional, and stabilized chronic stages will have an impact on the electric currents crossing the peri-electrode space in two directions, from the brain to the electrode in DBR procedures, and from the electrode to the brain in DBS procedures. Quantification of these effects would significantly enhance the capacity of investigating the biophysical mechanisms
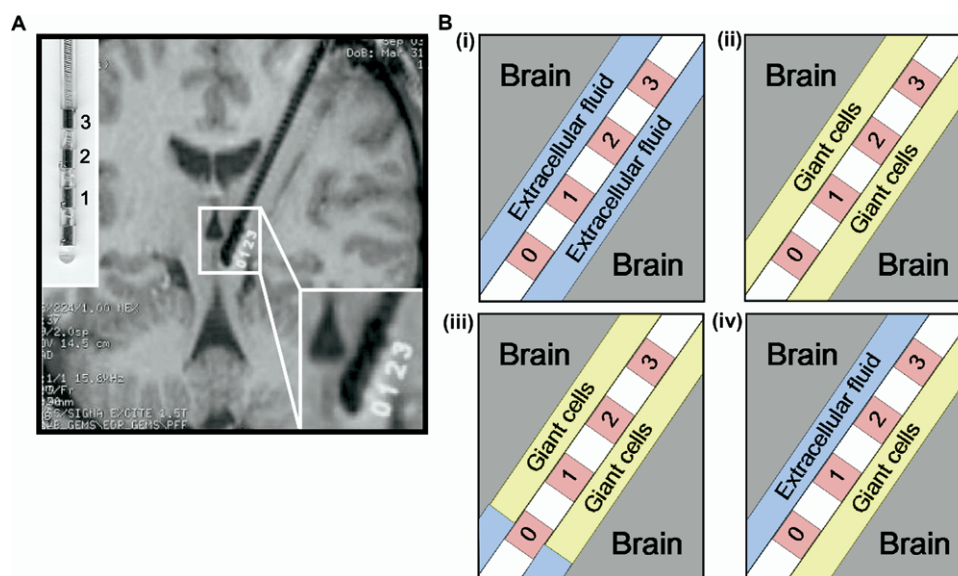
Fig. 1. Structural definition of the EBI: (A) an MRI of the implanted quadripolar DBS electrode *in situ*, with an enlarged photo of the electrode model 3387 (the left upper corner) and an enlargement of the EBI (the right lower corner), and (B) schematic representation of the EBI consisting of three essential elements of the implanted quadripolar electrode (contacts 0–3), the surrounding neural tissue, and the "peri-electrode space" in between, which is filled with ECF in the acute stage (i), with giant cells in the chronic stage (ii), and a mixture of ECF and giant cells in the transitional stages post-implantation. The giant cells grow transversely over all but the tip of the electrode (iii), or longitudinally over the lower half of the electrode (iv).

of DBR and DBS, of interpreting the recorded neural signals, of assisting the clinical adjustment of stimulation parameters, and of providing understanding of brain–computer interactions in general. In order to investigate the EBI at each of these stages it is necessary to take two complimentary approaches: for DBR during the acute stage, we recorded LFPs and correlated the amplitude changes of the modulated electrode potential with those of other physiological components in the compound LFP signals. For DBS we quantitatively compared the strength and distribution of the electric field generated by the stimulating current using computational simulations at the acute, transitional and chronic post-implantation stages, particularly as DBR is not common in the latter two stages post-implantation. Such a multi-disciplinary approach to investigating DBS has been shown to be valuable in past studies (Miocinovic et al., 2007).

EXPERIMENTAL PROCEDURES

Patients and physiological recordings

Approval of the local research ethics committee for recording, and written consent from patients was obtained. LFP signals were recorded from a total of 18 electrodes implanted in four subcortical regions including the STN (two electrodes), the medial globus pallidum (GP) (six), the motor (two) or sensory thalamus (three), and the periventricular gray (PVG) (five) in total 11 patients with either movement disorders including Parkinson's disease (one case), multiple sclerosis (one), essential tremor (one), myoclonus dystonia (one), generalized dystonia (two), or pathogenic central pain (five), who underwent therapy of chronic DBS. Detailed recording techniques have been previously reported (Xie et al., 2006; Wang et al., 2006) and are summarized here: LFPs were recorded via the implanted electrodes (model 3389/3387™; Medtronic Inc., Minneapolis, MN, USA) a few days after the initial electrode implantation. Simultaneous recordings of LFPs were made with three adjacent pairs of electrode contacts in a bipolar configuration. Signals were filtered between 0–1 kHz, amplified with a gain of ×10,000 (CED1902, Cambridge Electronic Design, Cambridge, UK). BP signals in all patients were simultaneously recorded using the non-invasive continuous finger arterial pressure monitor BP (Ohmeda Finapres2300, BOC Healthcare, NJ, USA). In five patients, simultaneous recording of LFP and BP signals was carried out while the patients performed short periods of exercise consisting of riding an exercise bicycle. The intensity of the exercise was controlled in order to increase the heart rate from a mean of 60 beats/min at rest, to just under 90 beats/min. All signals were digitized (CED1401mark II, Cambridge Electronic Design) at a sampling rate of 4000 Hz. As the main frequency range of interest in the present study is <10 Hz, all signals were filtered using a low-pass filter setting at 10 Hz. The time-frequency profile of the filtered LFP signals was obtained using short-time Fourier transform (STFT), time-window of 4 s with 2 s overlap; coherence and phase estimation was carried out using the same set of parameters (Wang et al., 2005). The statistical significance of the coherence estimates was tested using the independent threshold and the exact confidence interval (Wang et al., 2004). Linear regression was performed on the mean STFT power values over every 20 s between the LFP and BP signals in frequency, and significance of the correlation was statistically tested on the squared correlation coefficients value (r^2) at the level of probability 0.05. Cross-correlation was performed between the LFP and BP signals and the LFP and tidal volume signals. The 95% confidence interval of independence was calculated as 1.96 times of the standard error of the cross-correlogram. The chi-square test was used to statistically test the differences on electrode number of positive detection across the four brain regions. Computation and statistical analysis was carried out using MATLAB (v6.1, The MathWorks, Inc., MA, USA) and SPSS (v11, SPSS® Inc., Chicago, IL, USA).

The EBI and its structural FEM model

A detailed description of the structural EBI model was previously given (Yousif et al., 2007), and is summarized here: We used COMSOL Multiphysics 3.3 (COMSOL AB, Stockholm, Sweden) to form the EBI model. The EBI is defined by the description of the Medtronic 3389 electrode and the post-operative image of implanted electrode (Fig. 1A). A peri-electrode space is defined with an arbitrary thickness of 0.25 mm, which separates the implanted quadripolar electrode from the surrounding brain tissue of 10 mm radius (Fig. 1B). The model was meshed into 119,512 tetrahedral elements using a Delaunay meshing algorithm (COMSOL Multiphysics 3.3, COMSOL AB).

The potential distribution of the current injected via such an implanted electrode was obtained by solving Laplace's equation:

$$\nabla \cdot \sigma \nabla V = 0$$

where ∇ is the del operator and denotes the derivative of V in each of the (x, y, z) directions, V is the scalar potential (measured in volts), σ is the conductivity (measured in siemens per meter), and "." denotes a dot product. Therefore the model is quasi-static and does not account for time-varying currents, or the reactive component of the interface. As we focus on the properties of the EBI which are constant for all targets and disorders (Moss et al., 2004; Xie et al., 2006), we did not represent the detailed anatomy of a single DBS target, and hence the surrounding brain tissue was modeled as a homogenous cylinder of gray matter, with conductivity set at $\sigma_{tissue} = 0.2$ S/m (Geddes and Baker, 1967). To simulate monopolar stimulation, the active contact was set to −1 V, and the outer boundary of the surrounding tissue (which is 10 mm away from the surface of the electrode) was set to 0 V, both via Dirichlet boundary conditions ($V = V_0$, where V_0 is the specified value). The non-active contacts were bound using Neumann conditions ($n \cdot \nabla V = 0$, which fixes the normal derivative of the potential at the boundary).

Acute stage post-implantation

To simulate the EBI at the acute stage, during which the peri-electrode space is filled by ECF, we used the value of $\sigma_{ECF} = 1.7$ S/m (Rabbat, 1990) for this layer. All conductivity values used were robust, as doubling or halving only creates an average difference of <2% between percentage changes across conditions.

Chronic stage post-implantation

We also simulated the pathological growth of giant cells at the EBI, which has been shown previously to occur as early as 2 weeks post-implantation (Moss et al., 2004). This encapsulation tissue has been shown to be fibrous (Haberler et al., 2000; Henderson et al., 2002; Nielsen et al., 2007) and therefore we set the conductivity of the peri-electrode space at 0.125 S/m, which is equivalent that of white matter. This value is within the range measured for electrodes implanted in cats (Grill and Mortimer, 1994), and is consistent with values used in previous DBS modeling studies (Butson et al., 2006).

Transition stage post-implantation

A third time stage (relative to post-implantation) was simulated, which represents the transition between the acute stage when the peri-electrode space is filled with ECF, and the chronic stage

when the peri-electrode space is filled with giant cells. We simulated two possible spatial patterns of transition in 3D, one where giant cell growth occurs transversely over all but the tip of the electrode (Fig. 1B(iii)). The second involves giant cells growing longitudinally over half of the entire length of the electrode (Fig. 1B(iv)). These are two of the infinite number of possible spatial patterns of giant cell growth, and are used to simplify the more complex real situation.

Quantification

In order to quantify the effect of the changes at the EBI on the stimulation induced potential distribution, we measured the potential difference within the tissue, radially outwards at the level of contact zero, and approximated the distance at which neurons can be activated using a threshold of 0.5 V. This stimulation intensity value was determined based on our clinical practice of intraoperative monitoring during electrode implantation (Liu et al., 2005), during which we use this value for thresholding any induced therapeutic effect, such as tremor suppression following acute thalamic stimulation, and unwanted side effects, such as the capsular responses induced by direct activation of the pyramidal fibers.

RESULTS

Neurophysiological study of the physiological modulation of the EBI and the effect EBI on recorded neural signals via the implanted electrode

The general findings among a total of 18 electrodes implanted in four brain regions for treating different neurological conditions have been previously reported (Xie et al., 2006) and are summarized here: the modulated electrode potentials were clearly detected in 14 electrodes (77.5%) with a mean ($\pm$S.D.) peak-peak amplitude of 6.9$\pm$1.7 μV. No significant differences in detection rate (the GP 66%; the STN 100%; the thalamus 60%; the PVG 100%) and peak–peak amplitude (GP 4.6$\pm$1.6 μV; STN 7.0$\pm$2.9 μV; thalamus 9.4$\pm$5.2 μV; PVG 6.5$\pm$3.5 μV) were measured among the four brain regions.

In the present study, our results confirmed our previous finding that the electrode potential is modulated by brain pulsation *in situ* and is specifically related to the EBI. Significant linear correlation was found between the exercise-induced changes in heart rate and the frequency changes in the electrode potential over time ($r=0.93$, $n=76$, $P<0.0001$, Fig. 2). Furthermore, in all four brain regions tested, the changes in heart rate were correlated with the changes in the power value of the BP signal ($r=0.64$, $n=76$, $P<0.0001$), whereas the changes in the frequency were reversely correlated with the power value of the modulated electrode potential ($r=-0.26$, $n=76$, $P<0.05$). This suggests that exercise induces increases in blood perfusion to the brain in both rate and volume, and consequently increases the brain pulsation rate and the intracranial pressure. The former may be responsible for the simultaneous increase in frequency of the modulated electrode potential, and the latter reduces the magnitude of the modulated electrode potential, possibly resulting from the increase in tissue pressure on the electrode surface.

The effect of the modulation of the peri-electrode space by brain pulsation was directly investigated by cor-
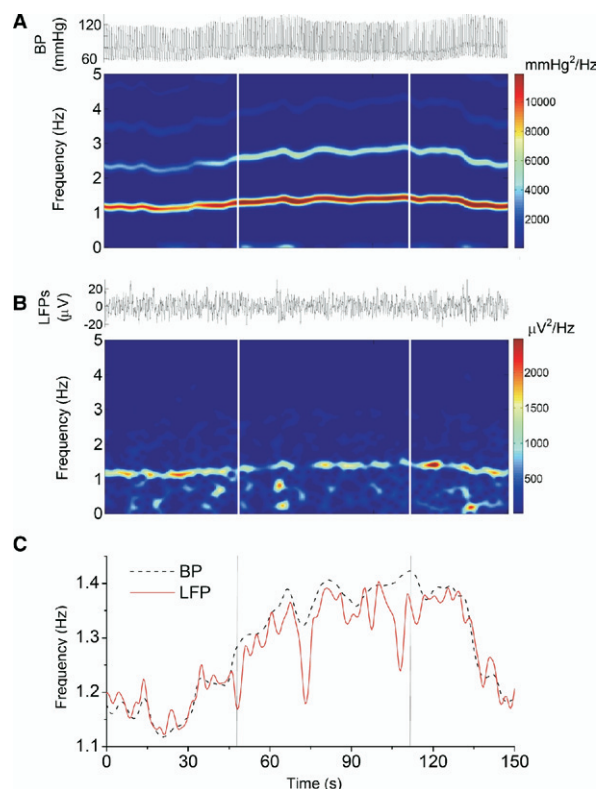

Fig. 2. Representative example of simultaneously recorded BP (A) and LFP (B) signals and their spectrograms over a period of mild exercise. The frequency change in BP signal induced by exercise significantly correlated with the changes in the frequency change in the electrode potential (C) over time. The onset and offset of the exercise are indicated by the vertical lines.

relating the amplitude of the modulated electrode potential with the amplitude of the oscillatory activity in the tremor (4–8 Hz) and beta (15–20 Hz) frequency bands in LFPs recorded from the subthalamic nuclei of a patient with Parkinson's disease (Fig. 3). Intriguingly, the increase in the amplitude of the modulated electrode potential is reversely correlated with the tremor oscillation ($r=-0.507$, $n=29$, $P<0.005$), but not the beta oscillation ($r=-0.01$, $n=29$, $P>0.5$). This may be the first direct evidence showing that the changes in the biophysical properties of the EBI under physiological conditions have selective effects on the neural signals crossing the EBI from the surrounding brain volume to the electrode contacts.

Computational study of the effect of the EBI on stimulation at different stages

In addition to the physiological study in the acute post-implantation stage, simulations were carried out with a focus on the transitional and chronic stages. The "shielding effect" of giant cells on the potential distribution was visualized by comparing the potential distribution around the activated electrode contact during monopolar settings when the peri-electrode space is filled with ECF (left, Fig. 4A), and when filled with giant cells (center, Fig. 4A). The spread of current was restricted by the low conductivity
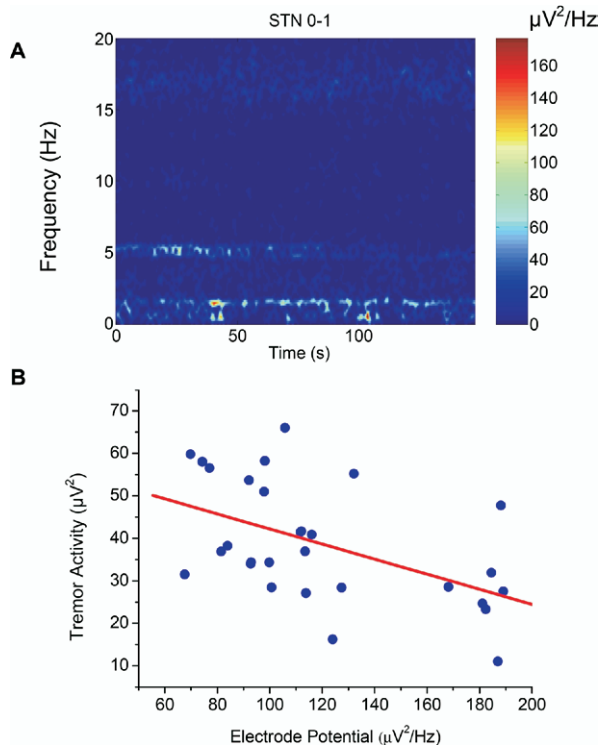
Fig. 3. Representative bipolar (contacts 0–1) LFP recording from the STN of a patient with parkinsonian tremor. (A) Three frequency components of the modulated electrode potential (1.0–1.5 Hz), tremor oscillation (4–6 Hz) and the beta oscillation (15–20 Hz) in the time-frequency spectrograms of compound LFPs; and significant reverse correlations in power density between the electrode potential and the tremor oscillation (B) but not the beta oscillation.

giant cells and consequently the magnitude of the potential at a given distance was consistently less than in the acute (ECF) case. To maintain the potential magnitude and compensate for giant cell growth, the stimulating intensity needed to be increased (right, Fig. 4A) from −1.0 V to −1.7 V (70%). To further illustrate the effect on field distribution of the "shielding effect," activation distance/stimulation intensity curves for both the acute and chronic cases were plotted (Fig. 4B). As one may expect, with the same stimulation intensity, the effective activation falls short by a distance ranging from 1.2 mm to 2.0 mm over the stimulation range of 0–10 V, suggesting that giant cell growth in chronic stages post-implantation significantly reduces the stimulation efficacy.

Simulating the changes during the transitional stage is more difficult, as there may be an infinite number of patterns of changes in the bio-physical properties of the peri-electrode space, as the giant cells may unevenly cover the electrode, e.g. top to bottom (left, Fig. 5A) or side to side (right, Fig. 5A). In comparison with the approximately spherical field distribution in the acute and chronic stages, during these transitional periods the field is distorted in shape and reduced in size depending on which part of and to what extent the ECF is replaced by the low-conductivity cells. We further quantified this change in the shape of the induced field, by plotting the two-dimensional region

around the electrode within which the induced potential distribution reaches the threshold of 0.5 V (Fig. 5B). These plots further indicate that during the transitional period, there will be a deviation away from a symmetric region of activated neural tissue, as induced in the acute stage.

DISCUSSION

By taking an approach which combines neurophysiological recording with computational modeling, the present study quantitatively demonstrated the impact of the peri-electrode space on the electric currents crossing the EBI in both DBR and DBS procedures over different stages post-implantation.

The results show that the electrode potential was modulated in amplitude by brain pulsation at the heart rate, as the recorded electrode potential was significantly correlated in frequency with the BP signal over a short period of gentle exercise, during which the heart rate increased physiologically (Xie et al., 2006). The modulation of the electrode potential in the acute stage may represent changes in the biophysical properties of the EBI in two possible ways: (1) during electrode implantation through craniotomy, the peri-electrode space may change its thickness due to increased pressure as cerebrospinal fluid flows away from the electrode tip along the electrode track; and (2) after implantation when the cranium is closed, brain pulsation may change the pressure of the tissue on the electrode surface. The most interesting physiological finding of the present study is that, perhaps for the first time, the effect of EBI modulation on the neural signals recorded via the implanted electrode has been quantitatively demonstrated by correlating the amplitude of the EBI-specific modulated electrode potential to the physiological signals in the tremor and beta frequency bands. As the physiological nature of the oscillatory STN LFPs in Parkinson's disease patients at the tremor and beta bands has been well established previously e.g. (Brown and Williams, 2005; Wang et al., 2006), the differential correlations in the amplitude of the modulated electrode potential with the tremor and beta oscillations revealed in the present study provide direct evidence that the changes in the biophysical properties of the EBI may have significant effects on the physiological signals crossing the depth EBI. The results show that the amplitude of the electrode potential was reversely correlated with the amplitude of the tremor oscillation (4–6 Hz) but not with the beta oscillation (15–20 Hz), suggesting that the effects of the EBI on the crossing physiological signals during recording may differentially relate to the frequency profile of the oscillations, as the low frequency *tremor oscillation* of a compound LFP signal is more susceptible to being "blocked." These results have two direct practical implications in DBR. Our previous study has shown that the amplitude of the electrode potential modulated by brain pulsation contributes to 30% of the overall peak to peak amplitude of the compound LFPs (Xie et al., 2006), and that the origin of this component could be simply ignored or misinterpreted if the biophysical structure of the EBI were not well understood.
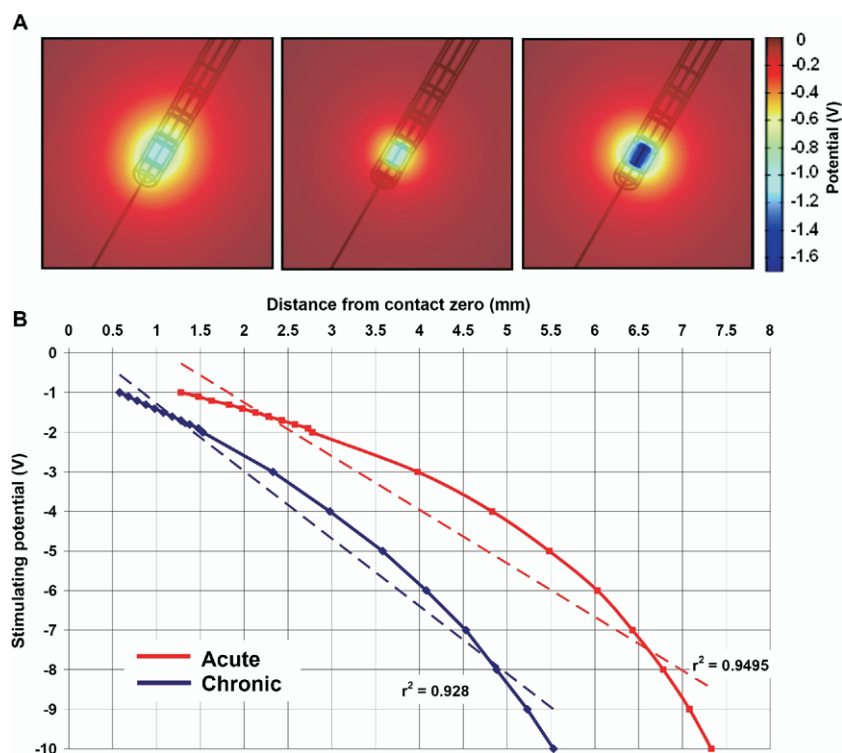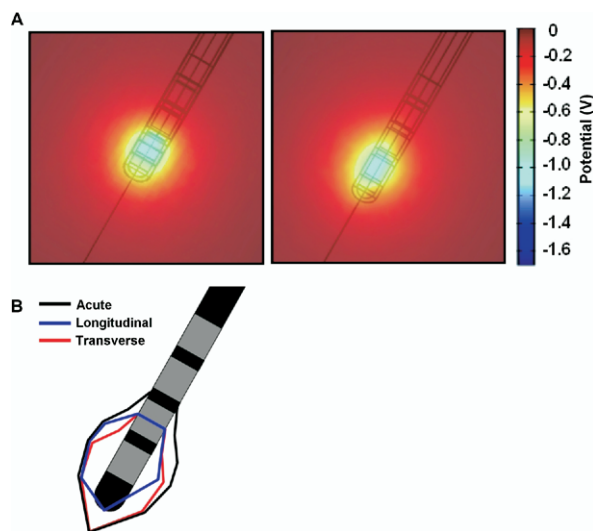
Fig. 4. Induced potential distribution when the peri-electrode space is filled with ECF (left, −1.0 V) and giant cells (center, −1.0 V), and compensatory increase in stimulating intensity of −1.7 V in the giant cell case (right, −1.7 V) to maintain the same level of stimulation as the ECF case. (B) Comparison of the estimated intensity-distance curves with an assumed activation threshold of 0.5 V between ECF and the giant cell cases.

Furthermore, in contrast to the electrode-tissue interface of large surface, high impedance electrodes, as used for recording scalp EEG, the present evidence suggests that the EBI of small surface, low impedance electrodes has a reactive in addition to a resistive component. One could

Fig. 5. Induced potential distribution at two possible transitional periods, when giant cells have grown transversely over all but the tip of the electrode (left), and longitudinally over half of the length of the electrode (right). (B) Comparison of the estimated region of neuronal tissue being activated by a threshold of 0.5 V between the acute and two putative transition cases.

reduce this reactive component by using better materials or improving the electrode design so that the effect of EBI on recording, particularly the low frequency component, can be reduced. For example, a recent modeling study suggested that such mechanical forces at the EBI could be reduced by the use of a hypothetical "soft" material, which is more flexible and has a larger elastic modulus (E=6 MPa) than traditionally used "stiff" materials such as silicon which has a relatively low elastic modulus (E=200 GPa) (Subbaroyan et al., 2005).

When it comes to investigating the effects of the EBI *in situ* on the injected current crossing the interface, neurophysiological investigation becomes almost impossible. Consequently, a physiologically plausible structural model of the EBI is a powerful tool, where *in vivo* measurement of the electric current in the surrounding brain volume cannot be measured directly. Based on our previously reported finite element EBI model (Yousif et al., 2007), we quantified the effect of the EBI on the injected current at the chronic stage, when the depth EBI is infiltrated by giant cells. Our simulations showed that the decline in potential intensity over space became more rapid than when ECF was present, suggesting a "shielding effect" on the stimulating current. Subsequently the range of the effective activation is reduced. In practice, an increase in DBS current intensity of between 70% and 100% was needed in order to fully compensate for the shortfall and maintain the same level of activation. A similar effect has been shown to occur for cochlear implants, as reviewed recently (Micco and Richter, 2006). One of the key results of the current

study, is to point out that there is a transitional period over the initial 2–8 weeks following implantation (Moss et al., 2004; Griffith and Humphrey, 2006), during which the ECF filled peri-electrode space is gradually replaced by the growth of the reactive giant cells. Partial "encapsulation" around the electrode contacts will change the shape and size of the stimulation induced electric field in an unpredictable pattern. These results may contribute to explaining the following clinical observations: (1) there is a gradual build-up of patient tolerance to stimulation during the initial a couple of weeks; (2) some stimulation side-effects due to over-activation are transient; and (3) there is a necessity for gradually increasing stimulation intensity during the initial a few weeks following electrode implantation (Kuncel et al., 2006), although the micro-lesioning effect of the electrode implantation may also play a role. Usually the need for the adjustment of stimulation parameters to achieve clinical improvement is reduced after 6–8 weeks, which may partially relate to the stabilization of the depth EBI. In this regard, the clinical significance of giant cell formation is limited. However, although the shortfall in the electric field distribution caused by giant cell growth or gliosis can be compensated for, and the therapeutic effect can be maintained by increasing the stimulation intensity, the energy consumption of the implantable pulse generator will also be increased so that the life expectancy of the stimulator battery is reduced and battery replacement becomes more frequent. Thus, there may be a need to minimize the reactive cell growth and the subsequent "shielding effect" by designing and manufacturing new electrodes.

There are some shortcomings in the simulations using the FEM model presented here. These have been discussed in detail in a recent review (Yousif and Liu, 2007b), and are also considered briefly here. The most obvious limitation is that the model derives the DBS induced potential distribution by solving Laplace's equation within a three-dimensional domain. Laplace's equation delivers an electrostatic solution which contains no temporal component. Therefore, this model is sub-optimal for simulating the dynamic nature of the stimulation pulses of various waveforms and frequencies. Our present results showed that the effects of EBI modulation on the passing neural signal were frequency dependent, such that the low frequency component is blocked more than the high frequency component in compound signals, suggesting that the EBI has a significant reactive in addition to resistive component. This reactive component is not accounted for in this static model, and therefore these shortcomings need to be overcome in future studies. However, the model used in the current study is robust and easy to achieve in terms of computing power, and it gives direct visualization of the distribution of the electric current, which is otherwise difficult to quantify. Furthermore, we tackled the limitation of a quasi-static approximation by quantifying the relative difference between the potential distributions induced at different time stages post-implantation. Consequently, as we have not explicitly commented on the absolute range of the field the use of quasi-static approximation is unlikely to

have affected our conclusions. However, an attempt has been made to introduce time dependence into FEM models by using a Fourier-FEM approach (Butson and McIntyre, 2005), and a 20% more accurate estimation of the volume of tissue activated was claimed.

CONCLUSION

In conclusion, using a combination of LFP recordings from implanted electrodes and computational simulations, the present study quantified the effects of the depth EBI on both recorded LFPs, and injected stimulation currents over three different post-implantation stages. Our results indicate that in acute conditions, the modulation of the fluid filled peri-electrode space affects currents crossing the EBI. This may not be significant for the stimulating current of a few volts in magnitude, but is clearly affecting the recorded LFP signal of a smaller magnitude of the order of tens of mV. In the transitional stage, until the EBI becomes stable, the combination of the reduction of the implantation-induced traumatic effect and the gradual growth of reactive giant cells, shields the surrounding tissue from the stimulating current with uncontrollable and transient changes in the shape and size of the electric field, which may contribute to the necessity of parameter adjustment in the initial few weeks post-implantation.

REFERENCES

Benabid AL, Benazzous A, Pollak P (2002) Mechanisms of deep brain stimulation. Mov Disord 17(Suppl 3):S73–S74.

Benabid AL, Pollak P, Gross C, Hoffmann D, Benazzouz A, Gao DM, Laurent A, Gentil M, Perret J (1994) Acute and long-term effects of subthalamic nucleus stimulation in Parkinson's disease. Stereotact Funct Neurosurg 62:76–84.

Benabid AL, Pollak P, Louveau A, Henry S, de Rougemont J (1987) Combined (thalamotomy and stimulation) stereotactic surgery of the VIM thalamic nucleus for bilateral Parkinson disease. Appl Neurophysiol 50:344–346.

Bittar RG, Otero S, Carter H, Aziz TZ (2005) Deep brain stimulation for phantom limb pain. J Clin Neurosci 12:399–404.

Brown P, Chen CC, Wang S, Kuhn AA, Doyle L, Yarrow K, Nuttin B, Stein J, Aziz T (2006) Involvement of human basal ganglia in offline feedback control of voluntary movement. Curr Biol 16:2129–2134.

Brown P, Mazzone P, Oliviero A, Altibrandi MG, Pilato F, Tonali PA, Di Lazzaro V (2004) Effects of stimulation of the subthalamic area on oscillatory pallidal activity in Parkinson's disease. Exp Neurol 188:480–490.

Brown P, Oliviero A, Mazzone P, Insola A, Tonali P, Lazzaro VD (2001) Dopamine dependency of oscillations between subthalamic nucleus and pallidum in Parkinson's disease. J Neurosci 21: 1033–1038.

Brown P, Williams D (2005) Basal ganglia local field potential activity: character and functional significance in the human. Clin Neurophysiol 116:2510–2519.

Butson CR, Cooper SE, Henderson JM, McIntyre CC (2007) Patient-specific analysis of the volume of tissue activated during deep brain stimulation. Neuroimage 34:661–670.

Butson CR, Maks CB, McIntyre CC (2006) Sources and effects of electrode impedance during deep brain stimulation. Clin Neurophysiol 117:447–454.

Butson CR, McIntyre CC (2005) Tissue and electrode capacitance reduce neural activation volumes during deep brain stimulation. Clin Neurophysiol 116:2490–2500.

Deuschl G, Schade-Brittinger C, Krack P, Volkmann J, Schafer H, Botzel K, Daniels C, Deutschlander A, Dillmann U, Eisner W, Gruber D, Hamel W, Herzog J, Hilker R, Klebe S, Kloss M, Koy J, Krause M, Kupsch A, Lorenz D, Lorenzl S, Mehdorn HM, Moringlane JR, Oertel W, Pinsker MO, Reichmann H, Reuss A, Schneider GH, Schnitzler A, Steude U, Sturm V, Timmermann L, Tronnier V, Trottenberg T, Wojtecki L, Wolf E, Poewe W, Voges J, the German Parkinson Study Group NS (2006) A randomized trial of deep-brain stimulation for Parkinson's disease. N Engl J Med 355:896–908.

Doyle LM, Kuhn AA, Hariz M, Kupsch A, Schneider GH, Brown P (2005) Levodopa-induced modulation of subthalamic beta oscillations during self-paced movements in patients with Parkinson's disease. Eur J Neurosci 21:1403–1412.

Engel AK, Moll CK, Fried I, Ojemann GA (2005) Invasive recordings from the human brain: clinical insights and beyond. Nat Rev Neurosci 6:35–47.

Foffani G, Ardolino G, Egidi M, Caputo E, Bossi B, Priori A (2006) Subthalamic oscillatory activities at beta or higher frequency do not change after high-frequency DBS in Parkinson's disease. Brain Res Bull 69:123–130.

Geddes LA, Baker LE (1967) The specific resistance of biological material: a compendium of data for the biomedical engineer and physiologist. Med Biol Eng 5:271–293.

Gimsa U, Schreiber U, Habel B, Flehr J, van Rienen U, Gimsa J (2006) Matching geometry and stimulation parameters of electrodes for deep brain stimulation experiments-numerical considerations. J Neurosci Methods 150:212–227.

Griffith RW, Humphrey DR (2006) Long-term gliosis around chronically implanted platinum electrodes in the Rhesus macaque motor cortex. Neurosci Lett 406:81–86.

Grill WM, Mortimer JT (1994) Electrical properties of implant encapsulation tissue. Ann Biomed Eng 22:23–33.

Haberler C, Alesch F, Mazal PR, Pilz P, Jellinger K, Pinter MM, Hainfellner JA, Budka H (2000) No tissue damage by chronic deep brain stimulation in Parkinson's disease. Ann Neurol 48:372–376.

Hemm S, Mennessier G, Vayssiere N, Cif L, Coubes P (2005a) Co-registration of stereotactic MRI and isofield lines during deep brain stimulation. Brain Res Bull 68:59–61.

Hemm S, Mennessier G, Vayssiere N, Cif L, El Fertit H, Coubes P (2005b) Deep brain stimulation in movement disorders: stereotactic coregistration of two-dimensional electrical field modeling and magnetic resonance imaging. J Neurosurg 103:949–955.

Henderson JM, Pell M, O'Sullivan DJ, McCusker EA, Fung VS, Hedges P, Halliday GM (2002) Postmortem analysis of bilateral subthalamic electrode implants in Parkinson's disease. Mov Disord 17:133–137.

Hillman EM (2007) Optical brain imaging in vivo: techniques and applications from animal to man. J Biomed Opt 12:051402.

Hodaie M, Wennberg RA, Dostrovsky JO, Lozano AM (2002) Chronic anterior thalamus stimulation for intractable epilepsy. Epilepsia 43:603–608.

Kerrigan JF, Litt B, Fisher RS, Cranstoun S, French JA, Blum DE, Dichter M, Shetter A, Baltuch G, Jaggi J, Krone S, Brodie M, Rise M, Graves N (2004) Electrical stimulation of the anterior nucleus of the thalamus for the treatment of intractable epilepsy. Epilepsia 45:346–354.

Kuhn AA, Kupsch A, Schneider GH, Brown P (2006) Reduction in subthalamic 8–35 Hz oscillatory activity correlates with clinical improvement in Parkinson's disease. Eur J Neurosci 23:1956–1960.

Kumar K, Toth C, Nath RK (1997) Deep brain stimulation for intractable pain: a 15-year experience. Neurosurgery 40:736–746.

Kuncel AM, Cooper SE, Wolgamuth BR, Clyde MA, Snyder SA, Montgomery EB Jr, Rezai AR, Grill WM (2006) Clinical response to varying the stimulus parameters in deep brain stimulation for essential tremor. Mov Disord 21:1920–1928.

Kupsch A, Benecke R, Muller J, Trottenberg T, Schneider GH, Poewe W, Eisner W, Wolters A, Muller JU, Deuschl G, Pinsker MO, Skogseid IM, Roeste GK, Vollmer-Haase J, Brentrup A, Krause M, Tronnier V, Schnitzler A, Voges J, Nikkhah G, Vesper J, Naumann M, Volkmann J, the Deep-Brain Stimulation for Dystonia Study Group (2006) Pallidal deep-brain stimulation in primary generalized or segmental dystonia. N Engl J Med 355:1978–1990.

Liu X (2003) What can be learned from recording local field potentials from the brain via implanted electrodes used to treat patients with movement disorders? Curr Med Lit Neurol 19:1–6.

Liu X, Aziz TZ, Bain PG (2005) Intraoperative monitoring of motor symptoms using surface electromyography during stereotactic surgery for movement disorders. J Clin Neurophysiol 22:183–191.

Liu X, Yianni J, Wang S, Bain PG, Stein JF, Aziz TZ (2006) Different mechanisms may generate sustained hypertonic and rhythmic bursting muscle activity in idiopathic dystonia. Exp Neurol 198:204–213.

Marceglia S, Foffani G, Bianchi AM, Baselli G, Tamma F, Egidi M, Priori A (2006) Dopamine-dependent non-linear correlation between subthalamic rhythms in Parkinson's disease. J Physiol 571:579–591.

Mayberg HS, Lozano AM, Voon V, McNeely HE, Seminowicz D, Hamani C, Schwalb JM, Kennedy SH (2005) Deep brain stimulation for treatment-resistant depression. Neuron 45:651–660.

McIntyre CC, Mori S, Sherman DL, Thakor NV, Vitek JL (2004) Electric field and stimulating influence generated by deep brain stimulation of the subthalamic nucleus. Clin Neurophysiol 115:589–595.

Micco AG, Richter CP (2006) Tissue resistivities determine the current flow in the cochlea. Curr Opin Otolaryngol Head Neck Surg 14:352–355.

Miocinovic S, Noecker AM, Maks CB, Butson CR, McIntyre CC (2007) Cicerone: stereotactic neurophysiological recording and deep brain stimulation electrode placement software system. Acta Neurochir Suppl 97:561–567.

Moss J, Ryder T, Aziz TZ, Graeber MB, Bain PG (2004) Electron microscopy of tissue adherent to explanted electrodes in dystonia and Parkinson's disease. Brain 127:2755–2763.

Nielsen MS, Bjarkam CR, Sorensen JC, Bojsen-Moller M, Sunde NA, Ostergaard K (2007) Chronic subthalamic high-frequency deep brain stimulation in Parkinson's disease: a histopathological study. Eur J Neurol 14:132–138.

Nuttin BJ, Gabriels LA, Cosyns PR, Meyerson BA, Andreewitch S, Sunaert SG, Maes AF, Dupont PJ, Gybels JM, Gielen F, Demeulemeester HG (2003) Long-term electrical capsular stimulation in patients with obsessive-compulsive disorder. Neurosurgery 52:1263–1272.

Pollo C, Villemure JG, Vingerhoets F, Ghika J, Maeder P, Meuli R (2004) Magnetic resonance artifact induced by the electrode Activa 3389: an in vitro and in vivo study. Acta Neurochir (Wien) 146:161–164.

Priori A, Ardolino G, Marceglia S, Mrakic-Sposta S, Locatelli M, Tamma F, Rossi L, Foffani G (2006) Low-frequency subthalamic oscillations increase after deep brain stimulation in Parkinson's disease. Brain Res Bull 71:149–154.

Priori A, Foffani G, Pesenti A, Tamma F, Bianchi AM, Pellegrini M, Locatelli M, Moxon KA, Villani RM (2004) Rhythm-specific pharmacological modulation of subthalamic activity in Parkinson's disease. Exp Neurol 189:369–379.

Rabbat A (1990) Tissue resistivity in electrical impedance tomography (Webster JG, ed). Bristol: Adam Hilger.

Rockwood AL (1986) Absolute half-cell thermodynamics: Electrode potential. Phys Rev A 33:554–559.

Sotiropoulos SN, Steinmetz PN (2007) Assessing the direct effects of deep brain stimulation using embedded axon models. J Neural Eng 4:107–119.

Subbaroyan J, Martin DC, Kipke DR (2005) A finite-element model of the mechanical effects of implantable microelectrodes in the cerebral cortex. J Neural Eng 2:103–113.

Thoma H, Gerner H, Holle J, Kluger P, Mayr W, Meister B, Schwanda G, Stohr H (1987) The phrenic pacemaker. Substitution of paralyzed functions in tetraplegia. ASAIO Trans 33:472–479.

Vidailhet M, Vercueil L, Houeto JL, Krystkowiak P, Benabid AL, Cornu P, Lagrange C, Tezenas du Montcel S, Dormont D, Grand S, Blond S, Detante O, Pillon B, Ardouin C, Agid Y, Destee A, Pollak P, the French Stimulation du Pallidum Interne dans la Dystonie (SPIDY) Study Group (2005) Bilateral deep-brain stimulation of the globus pallidus in primary generalized dystonia. N Engl J Med 352:459–467.

Vitek JL (2002) Mechanisms of deep brain stimulation: excitation or inhibition. Mov Disord 17(Suppl 3):S69–S72.

Wang S, Aziz TZ, Stein JF, Bain PG, Liu X (2006) Physiological and harmonic components in neural and muscular coherence in Parkinsonian tremor. Clin Neurophysiol 117:1487–1498.

Wang SY, Aziz TZ, Stein JF, Liu X (2005) Time-frequency analysis of transient neuromuscular events: dynamic changes in activity of the subthalamic nucleus and forearm muscles related to the intermittent resting tremor. J Neurosci Methods 145:151–158.

Wang SY, Liu X, Yianni J, Christopher MR, Aziz TZ, Stein JF (2004) Optimising coherence estimation to assess the functional correlation of tremor-related activity between the subthalamic nucleus and the forearm muscles. J Neurosci Methods 136:197–205.

Wingeier B, Tcheng T, Koop MM, Hill BC, Heit G, Bronte-Stewart HM (2006) Intra-operative STN DBS attenuates the prominent beta rhythm in the STN in Parkinson's disease. Exp Neurol 197:244–251.

Xie K, Wang S, Aziz TZ, Stein JF, Liu X (2006) The physiologically modulated electrical potential at the electrode-brain interface of deep brain stimulation in humans. Neurosci Lett 402:238–243.

Young RF, Chambi VI (1987) Pain relief by electrical stimulation of the periaqueductal and periventricular gray matter. Evidence for a non-opioid mechanism. J Neurosurg 66:364–371.

Yousif N, Bayford R, Bain PG, Liu X (2007) The peri-electrode space is a significant element of the electrode-brain interface in deep brain stimulation: A computational study. Brain Res Bull 74:361–368.

Yousif N, Liu X (2007a) Investigating the mechanisms of deep brain stimulation: computational modeling approaches: a commentary. Curr Med Lit Neurol 23:29–34.

Yousif N, Liu X (2007b) Modeling the current distribution across the depth electrode-brain interface in deep brain stimulation. Expert Rev Med Devices 4:623–631.

Zienkiewicz OC, Taylor RL, Zhu JZ (2005) The finite element method: Its basis and fundamentals, 6th edition. Butterworth Heinemen.